Hydrogen Storage Optimization in the T Gas Field: Numerical Simulation Insights from the Ordos Basin

Xueling Ma, **Lu Zou**, **Zhanrong Yang**, **Tong Hou**, **Weirong Li***, Xi'an Shiyou University, Xi'an, China; **Keze Lin**, China University of Petroleum, Beijing, China; **Hongliang Yi**, Liaohe Oilfield, CNPC, China; **Zhilong Liu**, CNOOC Energy Technology & Services Limited, Tianjin, China

Abstract

Amidst the global acceleration of the energy transition and the widespread adoption of renewable energy, hydrogen has emerged as a cornerstone of future energy systems, owing to its zero-carbon emissions and high energy density. Nevertheless, the pursuit of efficient large-scale hydrogen storage persists as a formidable challenge. This research employs numerical simulations to comprehensively analyze underground hydrogen storage (UHS) in the depleted T gas field within the Ordos Basin, China. A detailed geological model and a PVT (Pressure-Volume-Temperature) fluid model encompassing hydrogen, methane, and other gases were meticulously developed. The study systematically investigated multiple factors, including hydrogen injection timing, injection rate, injection-production cycles, buffer gas type, and molecular diffusion, to assess their effects on hydrogen storage and recovery. The findings confirm that depleted gas reservoirs are highly suitable for ultra-high- pressure hydrogen storage, with a remarkable hydrogen recovery rate reaching 92.15%. It was emphasized that residual gas saturation (linked to injection timing) and buffer gas type significantly influence hydrogen purity and the ultimate recovery rate. Nitrogen, when used as a buffer gas, can enhance hydrogen recovery. Additionally, molecular diffusion was found to cause a 3.3% reduction in hydrogen recovery at lower injection rates. The research also revealed that although higher injection rates may lead to a decrease in hydrogen recovery, the number of injection-production cycles has a negligible impact on recovery performance. This in-depth exploration of ultra-high-pressure hydrogen storage in depleted gas fields identifies key variables and offers valuable insights for optimizing the deployment and operational efficiency of this technology.

Introduction

The global energy landscape is undergoing a paradigm shift driven by industrialization, urbanization, and escalating demand for sustainable solutions. While fossil fuels remain the primary energy source for most nations, concerns over energy security, greenhouse gas emissions, and environmental degradation have intensified efforts to transition toward renewable energy systems (Zhu 2021). Countries such as the United States, China, Germany, and Australia have implemented national strategies to prioritize investments in wind, solar, and hydropower technologies, aiming to reduce reliance on coal and nuclear energy (Noussan et al. 2021; Bauer et al. 2022).

Hydrogen, the most abundant element in the universe, has emerged as a cornerstone of decarbonization due to its high gravimetric energy density and zero-carbon emissions upon combustion (Gabrielli et al. 2020). With declining costs of renewable electricity, electrolytic hydrogen production has become economically viable, positioning hydrogen as a versatile energy carrier for transportation, heating, and power generation (Li et al.

Improved Oil and Gas Recovery

DOI: 10.14800/IOGR.1370

Received January 17, 2025; revised February 1, 2025; accepted February 14, 2025.

*Corresponding author: weirong.li@hotmail.com

2021; Shao and Yi 2019). However, the intermittent nature of renewable energy sources introduces supply volatility, necessitating large-scale storage solutions to ensure grid stability and seasonal energy security (Shi et al. 2020; Züttel 2003).

Conventional hydrogen storage methods — including high-pressure cylinders, cryogenic liquefaction, and adsorption via metal hydrides or nanomaterials—face limitations in cost, volumetric efficiency, and reversibility (Zhou 2005; Demirel 2012). For instance, compressed gas storage at 800 bar incurs high capital costs, while cryogenic systems require energy-intensive liquefaction at 21 K (Züttel 2004). Metal hydrides and chemisorption-based approaches suffer from low gravimetric capacity (<3 wt%) and kinetic constraints (Hagemann et al. 2018). Consequently, subsurface storage in geological formations, such as salt caverns, aquifers, and depleted hydrocarbon reservoirs, has gained traction as a scalable and cost-effective alternative (Thoraval et al. 2015).

Salt caverns, though mature for hydrogen storage, demand specific halite deposits and multiyear development timelines for leaching (Michalski et al. 2017; Ozarslan, 2012). Aquifers require structurally intact caprocks, high permeability, and hydrodynamic traps to mitigate buoyancy-driven hydrogen migration (Kanaani et al. 2022). Depleted gas reservoirs, by contrast, offer inherent advantages: pre-existing infrastructure, proven sealing mechanisms, and residual methane cushion gas to minimize hydrogen mixing and enhance recovery (Zamehrian and Sedaee 2022; Tarkowski 2019). Additionally, hydrogen's lower solubility in natural gas compared to crude oil reduces operational losses, making gas reservoirs preferable to oil fields for storage (Amid et al. 2016).

Recent numerical and experimental studies have advanced understanding of hydrogen behavior in subsurface systems. Amid et al. (2016) demonstrated comparable working gas capacities for seasonal hydrogen and methane storage in depleted reservoirs. Hemme and Van Berk (2018) quantified minimal hydrogen losses (<2%) from microbial activity and diffusion in sandstone reservoirs. Lysyy et al. (2021) achieved 87% hydrogen recovery in the Norne Field via cyclic injection, highlighting the efficacy of residual methane as cushion gas. Carchini et al. (2023) further validated low hydrogen adsorption on calcite and silica surfaces, confirming the suitability of carbonate and siliciclastic reservoirs for storage.

Despite these advances, no prior studies have evaluated hydrogen storage potential in the Ordos Basin, China's second-largest sedimentary basin. The T Gas Field, located in the basin's stable cratonic setting, features a gently monoclinal structure, well-connected pore networks, and high reservoir continuity—attributes critical for minimizing hydrogen leakage and ensuring operational integrity (Mei 2011). Seasonal surpluses of wind and solar energy in western China (1.213 billion kW installed capacity by 2022) further underscore the strategic value of converting excess electricity to hydrogen for subsurface storage, thereby mitigating grid intermittency (Reuß et al. 2017; Gabrielli et al. 2020).

This study employs numerical simulation to assess the feasibility of hydrogen storage in the T Gas Field's depleted reservoirs. Section 2 details the simulation methodology, including reservoir characterization, fluid modeling, and operational constraints. Section 3 evaluates hydrogen injectivity, withdrawal efficiency, and parametric sensitivities (injection rate, cycle duration, cushion gas composition, and diffusion effects). Section 4 synthesizes key findings and implications for industrial deployment.

Establishment of Numerical Simulation Model

This study utilized the commercial numerical simulation software CMG to perform numerical simulations of an underground hydrogen storage system within a partially depleted natural gas reservoir in the T depleted gas field of the Ordos Basin, China. GEM, a pre- eminent equation of state (EOS) reservoir simulator, is well - suited for simulating multi-component systems, chemical flooding processes, gas storage scenarios, and unconventional reservoirs. Leveraging its advanced solver and parallel computing technology, GEM can fully exploit the hardware's capabilities to expedite the completion of large - scale, intricate simulation tasks. The fluid models were characterized using CMG's WINPROP software.

Reservoir Model. **Table 1** presents a comprehensive summary of the reservoir properties of the T gas field, encompassing parameters such as size, grid block dimensions, permeability, porosity, pressure, temperature, and saturation. The gas reservoir covers an area of approximately 1.8 km×1.9 km and was discretized into a 35×36×46 grid cell system along the x, y, and z directions, respectively.

A dual - well system, consisting of one injection well and one production well, was adopted for several key reasons. Firstly, it enables the coverage of a larger reservoir area. Secondly, it allows for effective control of the pressure distribution within the reservoir, thereby preventing reservoir damage that could result from excessively high or low pressures. This approach also helps maintain reservoir integrity and optimal hydrogen storage performance while ensuring a distinct division of roles between the injection and production wells.

The reservoir structure is depicted in **Figure 1**, where different grid colors represent varying reservoir depths, with the depth gradually increasing from blue to red. At the onset of hydrogen storage operations, the average reservoir pressure was 7 MPa. The rock compressibility was measured at 1×10^{-5} kPa^{-1}, and the reservoir is located at a depth of 2000 meters with a thickness of 430 meters. **Figure 2** illustrates the relative permeabilities of the water and gas phases within the reservoir matrix.

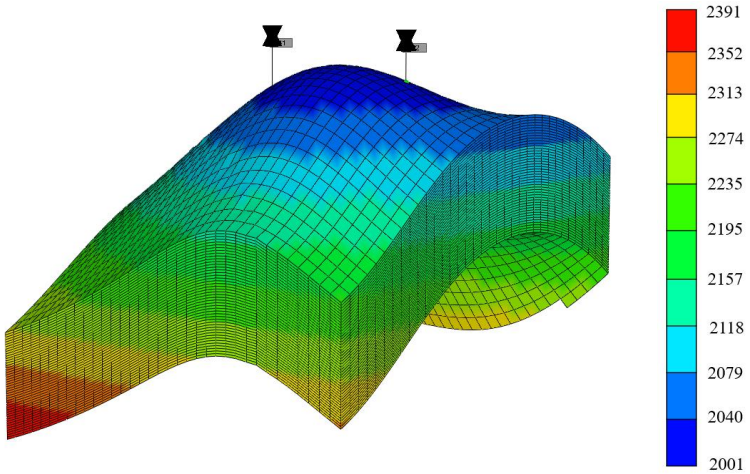

Figure 1—Geologic model.

Table 1—The Properties of reservoir model.

Parameters	Values
Number of grid blocks (i, j, k)	(35, 36, 46)
Grid block size, m×m×m	20×20×9.35
Reservoir depth, m	2000
Initial reservoir temperature,℃	80
Initial reservoir pressure at the grid top, kPa	2000
Mean permeability, mD	1.3
Porosity, %	20
Initial gas saturation, %	70
Initial water saturation, %	30

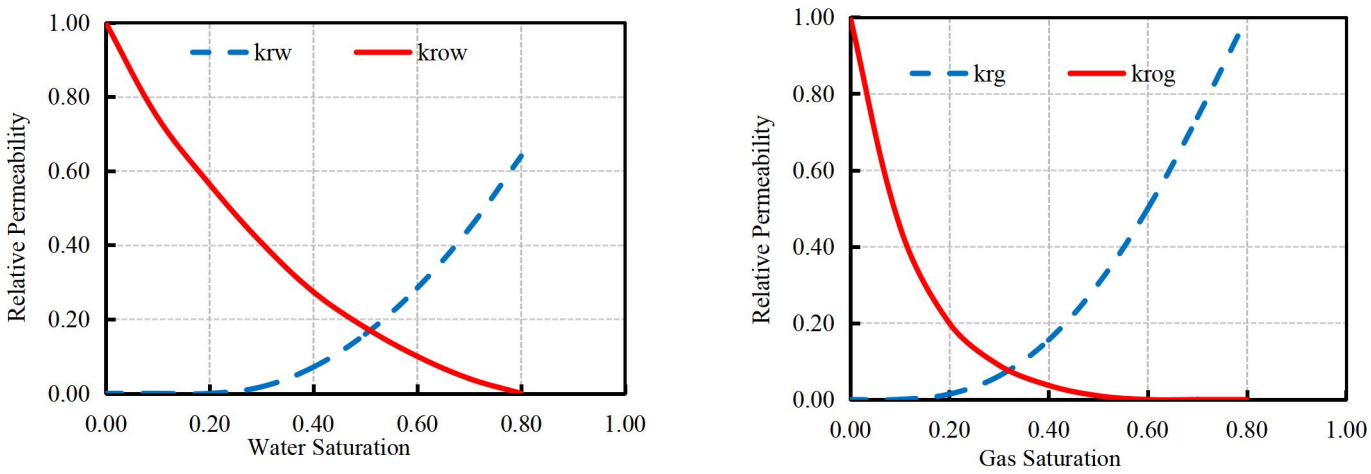

Figure 2—Relative permeability curve.

Fluid Model. In this research, only CH_4 was considered as the original fluid component in the T gas field. **Table 2** summarizes the fluid components, and their properties generated during the injection and production processes. The GEM module in the CMG software already incorporates the basic properties of H_2, N_2, CH_4, and CO_2.

H_2 serves as the primary component of the injected gas. Prior to H_2 injection, a combination of H_2, N_2, CO_2, and CH_4 is used as cushion gas. The cushion gas fulfills two main functions. Firstly, it pressurizes the reservoir to sustain the desired production rate. Secondly, it acts as a barrier between H_2 and the natural fluids in the reservoir. Therefore, meticulous consideration must be given to the type, volume, injection rate, and composition of the cushion gas, as the compatibility between the cushion gas and the existing fluids is critical in preventing unwanted chemical reactions. Moreover, since some cushion gases are expected to co - produce with H_2, the separation process also needs to be carefully considered.

Table 2—Component fluid system and parameters.

Component	Specific Gravity	Mole Weight, g/mol	Pc, atm	Tc, K	Acentric Factor	Composition, %
H_2	0.071	2.0159	12.9	33.19	0.214	0.0
N_2	0.967	28.013	33.5	126.2	0.04	0.0
CO_2	1.519	44.01	72.8	304.2	0.225	0.0
CH_4	0.553	16.043	45.4	190.6	0.008	1.0

Hydrogen gas is characterized by its colorless, odorless, highly flammable nature and strong reducing properties. It has low solubility in water. Compared to air, the relative molecular mass of H_2 is merely 0.069 times that of air, and it requires a compression capacity 14.5 times greater than that of air to achieve mass balance. At standard conditions, the density of H_2 (0.089 kg/m³) is approximately one - fourteenth of the density of air (1.29 kg/m³). The dynamic viscosity of air at standard conditions is 18.448×10^{-3} mPa·s, which is twice the dynamic viscosity of H_2 at 8.915×10^{-3} mPa·s. **Table 3** presents a summary of the physical and chemical properties of H_2 gas at standard conditions.

Table 3—Physical and chemical properties of H_2 at STP.

Properties	Unit	Values
Mole mass	/	2.016
Density (25°C, 1atm)	kg/m^3	0.08375
Calorific value	KJ/g	120-142
The concentration range of combustion in air	vol%	4-75
Minimum ignition energy	mJ	0.02
Self-ignition point	°C	585
Combustion heat	kcal/g	34.2
Diffusion coefficient in air (25°C, 1atm)	m^2/s	0.61×10^{-4}
Diffusion coefficient in pure water (25°C)	m^2/s	5.13×10^{-9}
Diffusion coefficient in clay saturated with water (25°C)	m^2/s	3.0×10^{-11}
Dynamic viscosity (50℃, 20MPa)	mPa·s	0.00935
Critical pressure	MPa	1.28
Critical temperature	°C	-239.95

The density of H_2 exhibits a sharp increase with rising pressure and a slight decrease with increasing temperature, as shown in **Figure 3(a)**. At a temperature of 298 K, when the pressure increases from 0.6 MPa to 16 MPa, the density of hydrogen gas rises from 0.5 kg/m³ to 12 kg/m³. At 30 MPa, as the temperature increases from 313 K to 373 K, the density of H_2 only decreases from 20 kg/m³ to 16 kg/m³.

The viscosity of hydrogen gas is minimally influenced by temperature and pressure, as depicted in **Figure 3(b)**. At 373 K, when the pressure increases from 0.1 MPa to 50 MPa, the viscosity of H_2 increases from 10.4×10^{-3} mPa·s to 11.8×10^{-3} mPa·s. At 20 MPa, as the temperature rises from 313 K to 373 K, the viscosity of hydrogen gas increases from 9.32×10^{-3} mPa·s to 10.31×10^{-3} mPa·s. According to Pan et al. (2021), high - pressure reservoirs offer greater storage potential for H_2 compared to atmospheric - pressure reservoirs when selecting geological spaces for hydrogen storage in depleted gas reservoirs.

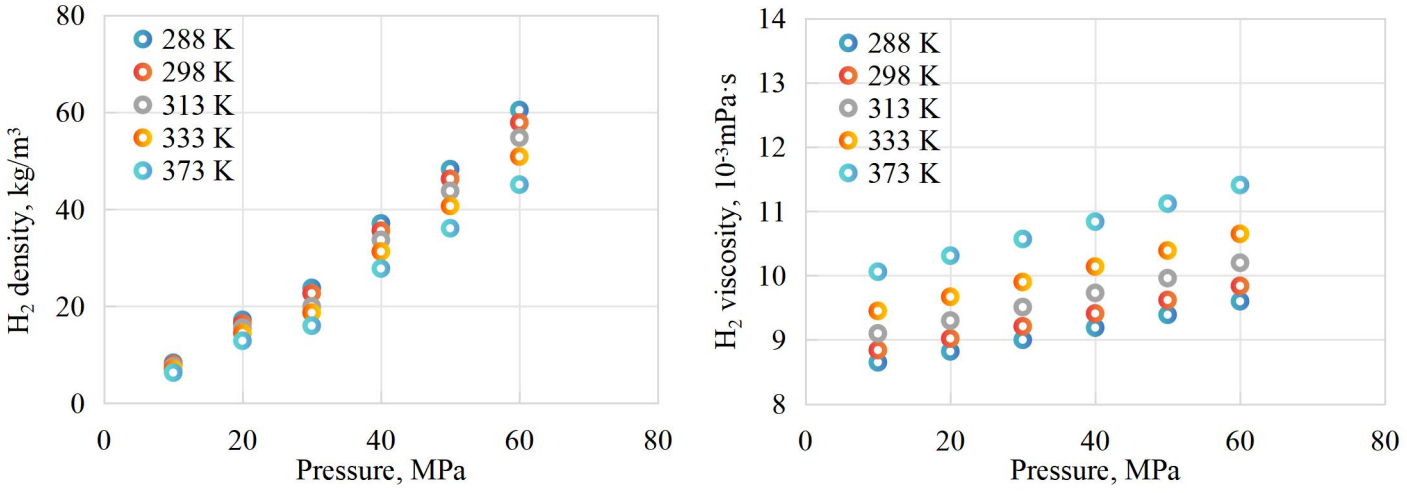

Figure 3—Relationship between gas (H_2) properties and pressure (Pan et al. 2021).

The diffusion coefficient of hydrogen gas is significantly affected by temperature and pressure, depending on the diffusion medium type, as shown in **Figure 4**. At 323 K, as the pressure increases from 0.35 MPa to 2.1 MPa, the diffusion coefficient of H_2 in CH_4 decreases from 1120 $\times 10^{-8}$ m²/s to 385 $\times 10^{-8}$ m²/s, nearly a three-fold reduction. In water at 25 MPa, as the temperature increases from 650 K to 973 K, the diffusion coefficient of H_2 increases from 14.4$\times 10^{-8}$ m²/s to 218.8$\times 10^{-8}$ m²/s (Pan et al. 2021).

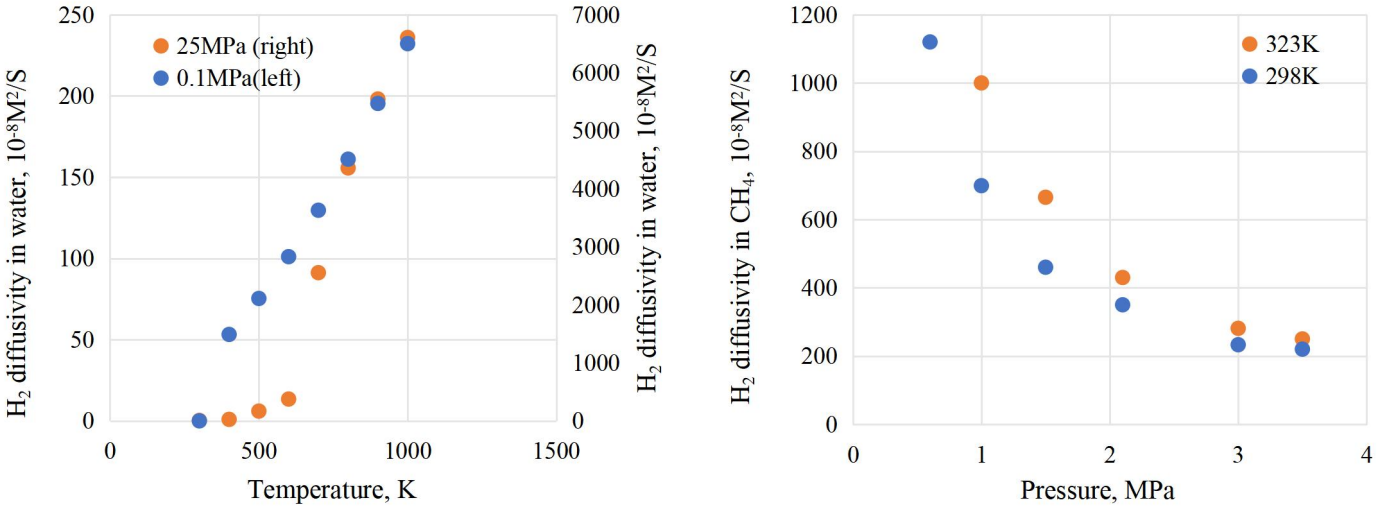

a. H_2 diffusivity in water b. H_2 diffusivity in CH_4

Figure 4—Relationship between H_2 diffusivity and pressure (Pan et al. 2021).

Simulation Settings for the Underground Hydrogen Storage (UHS). **Table 4** provides a summary of the well-controlled conditions for the underground hydrogen storage simulation. Throughout the entire production process, the depletion of gas production commences and continues until the average reservoir pressure drops to 7 MPa, corresponding to a maximum gas recovery of 65%. Subsequently, the underground hydrogen storage process is initiated.

Table 4—Simulation schemes.

		Parameter	UHS
Well control condition	Injection well	Max BHP, kPa	30000
		Gas injection rate, $\times 10^6 m^3$/day	1
	Production well	Min BHP, kPa	5000
		Initial stage gas Production rate, $\times 10^6 m^3$/day	0.4
		Period gas production rate, $\times 10^6 m^3$/day	2
Cycle index/Cycles			10
Gas injection cycle number/month			6
Gas production cycle number/month			3

The total production period spans 30 years, with the first 16 years dedicated to depletion gas production, followed by 7 years of hydrogen storage, and the final 7 years serving as an extended production period. The number of underground hydrogen storage cycles was set to 10, with each cycle consisting of 6 months of gas injection and 3 months of gas production.

The initial gas production rate is 0.4×10^6 m³/day. Drawing on previous research by Lysyy et al. (2021) and Mohammad et al. (2022), the gas injection time is designed to be twice the gas production time. Consequently, the gas production rate in the subsequent cycles is also twice the injection rate. The injection rate for H_2 remains consistently at 1×10^6 m³/day, while the gas production rate is 2×10^6 m³/day. During the initial depletion production process, the bottom - hole pressure (BHP) at the production well is set at 5000 kPa.

Additionally, a sensitivity analysis was conducted to evaluate the influence of injection timing, injection - production cycles, injection rates, molecular diffusion, and various cushion gases on the underground hydrogen storage process. **Table 5** summarizes the range of values for different influencing factors.

Table 5—Range of values for sensitivity analysis.

Influence factor	Range of values				
Injection timing (Pressure drops to, MPa)	7	10	13	16	19
Injection-production cycles	5	10	15	20	-
Injection rates, 10^6 m³/day	0.5	1	1.5	2	2.5
Molecular diffusion	Without diffusion			With diffusion	
Cushion gas	Without cushion gas	H_2	N_2	CH_4	CO_2

Results and Discussion

Base case underground hydrogen storage. After multiple simulations and sensitivity analyses, the underground hydrogen storage scheme was implemented as the gas reservoir pressure declined from 20MPa to 7MPa. Ten injection-production cycles were simulated, followed by a 7-year extended production period. Figure 6 illustrates the variations in reservoir pressure, hydrogen injection, and production during the hydrogen storage process. It's worth noting that the base case did not involve cushion gas injection. During the hydrogen storage process, the pressure gradually increases. As the initial reservoir pressure is relatively low (7 MPa), the volume of produced gas is significantly less than the amount of hydrogen injected. After each production cycle, the pressure does not return to its previous level. With subsequent alternating injections and production cycles, the pressure gradually increases, and the H_2 production increment becomes larger after each cycle. Since pure H_2 is injected, the mixture of hydrogen and methane is produced. As shown in Figure 7, the mole fraction of methane in the produced gas decreases after each cycle. Until the H_2 injection is stopped, the proportion of H_2 in the produced gas decreases, while the proportion of methane increases.

As shown in **Figure 5**, at the first, fifth, and tenth cycles, the cumulative amount of H_2 injected reached 3.62×10^8 m³, 18.2×10^8 m³, and 36.2×10^8 m³, respectively. Over the first, fifth, and tenth cycles, a cumulative amount of 1.19×10^8 m³, 10.82×10^8 m³, and 26.92×10^8 m³ of H_2 was recovered (**Table 6**). Finally, after a 7-year extended production period, the cumulative H_2 production could reach 33.36×10^8 m³. Due to the low energy in the early cycles, the reservoir pressure is insufficient, causing some H_2 to remain trapped in the reservoir and not be effectively recovered.

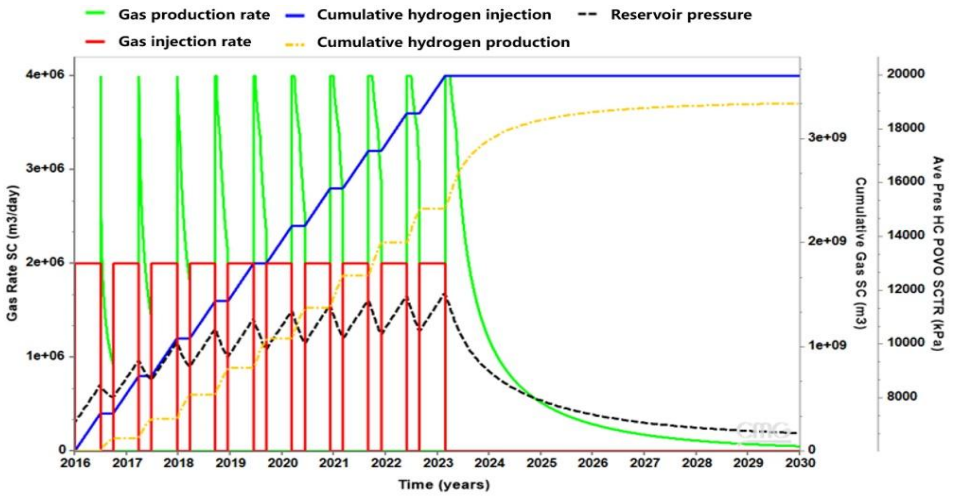

Figure 5—H_2 injection/production and reservoir pressure profile during UHS (basic case).

Additionally, as shown in **Figure 6**, the presence of methane further reduces the purity and recovery rate of H_2, as these fluids mix with H_2 or impede its flow. In each cycle, the trapped H_2 provides additional energy to the reservoir, and as the number of cycles increases, the reservoir pressure gradually recovers, while the amount of methane in the reservoir decreases. This process improves the flow and recovery efficiency of H_2, enhancing both its purity and recovery rate. However, once H_2 injection stops, the purity of hydrogen begins to decline.

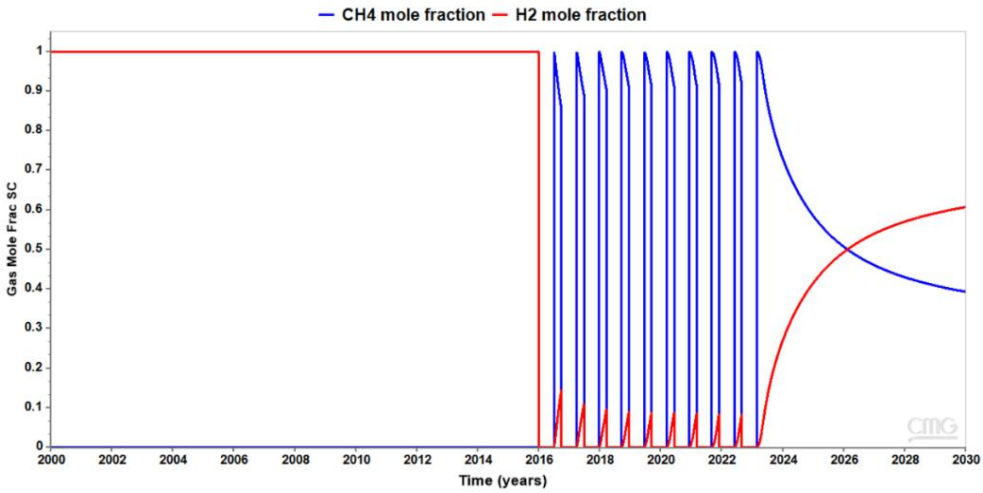

Figure 6—Mole fraction of the produced gas.

Additionally, the presence of methane further reduces the purity and recovery rate of H_2, as these fluids mix with H_2 or impede its flow. In each cycle, the trapped H_2 provides additional energy to the reservoir, and as the number of cycles increases, the reservoir pressure gradually recovers, while the amount of methane in the reservoir decreases. This process improves the flow and recovery efficiency of H_2, enhancing both its purity and recovery rate. However, once H_2 injection stops, the purity of hydrogen begins to decline.

After the completion of 10 injection-production cycles, the recovery for H_2 reaches 74.36%. The final recovery for H_2 is 92.15%. The final recovery of H_2 is determined by the extended production period because H_2 injection has ceased. To maximize economic benefits, it is necessary to evaluate the duration of the extended production period.

Table 6—H_2 recovery of UHS in basic case.

Cycle index	Frist cycle		5th cycle		10th cycle		Ultimate time		CH_4 EGR (%)
	CHP (10^8m^3)	H_2 RF (%)	CHP (10^8m^3)	H_2 RF (%)	CHP (10^8m^3)	H_2 RF (%)	CHP (10^8m^3)	H_2 RF (%)	
Value	1.19	32.87	10.82	59.45	26.92	74.36	33.36	92.15	6.34

(CHP: cumulative H_2 production; RF: H_2 recovery; Ultimate time: 7-year depletion phase following the final cycle)

Injection Time. The timing of implementing the underground hydrogen storage scheme is related to the degree of reservoir depletion. The longer the reservoir has been in production, the more depleted it becomes, resulting in lower reservoir pressure, which can affect the effectiveness of H_2 storage. To investigate the impact of the timing of hydrogen injection on underground hydrogen storage, simulations were designed for five groups of reservoirs with varying degrees of depletion. The degree of reservoir depletion is characterized by the extent of pressure drop in the reservoir.

Figure 7 shows the changes in reservoir pressure during hydrogen injection across various degrees of depletion. It is evident that as the depletion level intensifies, the increase in pressure becomes less significant. When the reservoir is minimally depleted, early hydrogen injection leads to a higher final H_2 recovery rate (**Table 7**). This is primarily because the original fluids within the reservoir help maintain pressure. Once these fluids are extracted, the reservoir loses some of its supportive pressure. Therefore, in gas reservoirs where the pressure has already decreased to lower levels, the newly injected H_2 struggles to attain the previously high-pressure states due to a lack of sufficient initial pressure. Moreover, as fluids are extracted, structural changes may occur in the reservoir, such as reduced porosity and the closure of fractures, further limiting the effective storage of H_2.

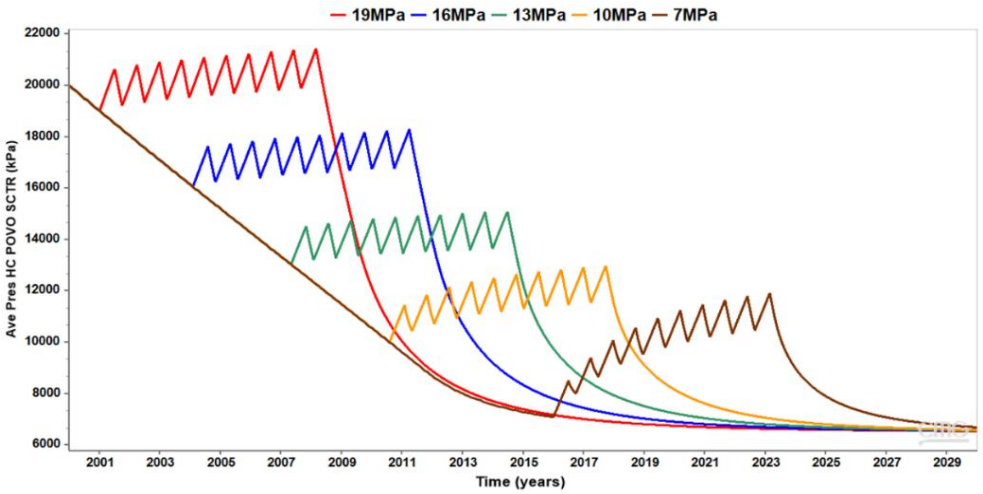

Figure 7--Effect of reservoir depletion degree on pressure profile during UHS.

Table 7--Effect of reservoir depletion degree on H_2 recovery.

Pressure (MPa)	10th cycle		Ultimate time	
	CHP (10^8m^3)	RF (%)	CHP (10^8m^3)	RF (%)
7	26.92	74.36	33.36	92.15
10	31.12	76.49	35.12	97.02
13	31.55	82.40	35.65	98.48
16	30.84	83.12	35.82	98.95
19	30.62	80.97	35.89	99.14

(CHP: cumulative H_2 production; RF: H_2 recovery; Ultimate time: 7-year depletion phase following the final cycle)

Figure 8 illustrates the molar fractions of methane within reservoirs at various depletion levels. The gas in the reservoir is a mixture of H_2 and CH_4. It is observed that higher reservoir pressures, corresponding to lower depletion levels, result in a larger amount of remaining CH_4. As a result, the CH_4 produced is of higher purity, while the purity of H_2 is lower, which entails additional costs for H_2 purification. Therefore, the timing of H_2 injection must balance between enhancing H_2 recovery and maintaining its purity.

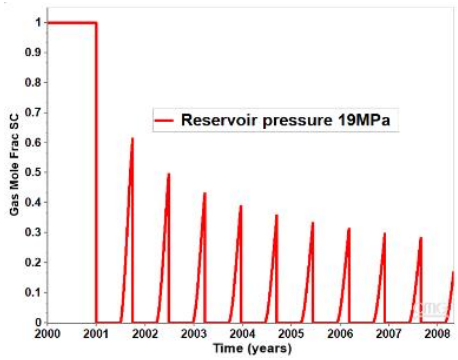

(a) 19MPa

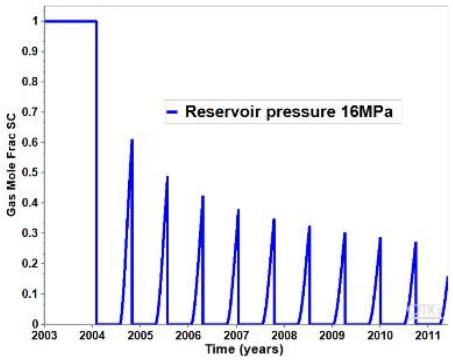

(b)16MPa

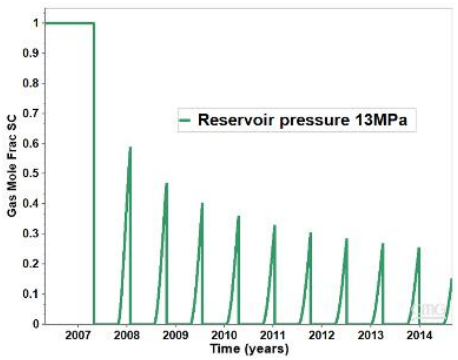

(c)13MPa

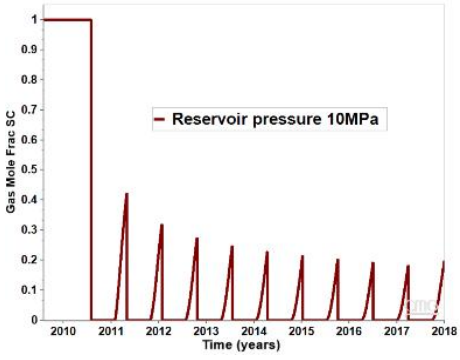

(d)10MPa

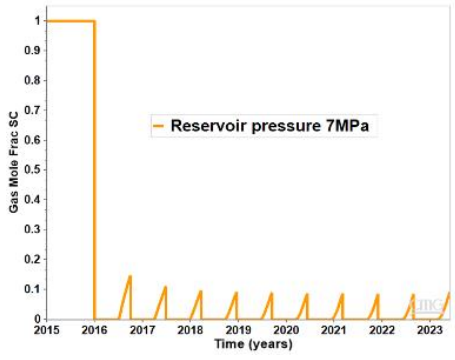

(e)7MPa

Figure 8—Mole fraction of CH_4 in different reservoirs pressure.

Different Cushion Gas. Injecting gas before injecting H_2 into the gas reservoir will increase the reservoir pressure and can mitigate the influence of gravity, thereby improving H_2 recovery. This study investigated the impact of injecting N_2, CH_4, H_2, and CO_2 as cushion gas on hydrogen storage. Each type of cushion gas was injected for 1 year at a rate of 1×10^6 m³/day.

As shown in **Figure 9**, using H_2 as a cushion gas results in the highest increase in reservoir pressure, reaching up to 9.95 MPa, followed by N_2 (9.75 MPa) and CH_4 (9.49 MPa). When CO_2 is used as a cushion gas, the pressure increases up to 9.01 MPa. These variations are attributed to the differences in specific gravities of the gases, which affect their gravitational segregation and buoyancy effects in the reservoir. Gases with high specific gravity, such as CO_2, tend to settle at the bottom of the reservoir, thereby reducing the height of the gas column and contributing less to the pressure increase. Conversely, gases with low specific gravity, such as H_2 and N_2, distribute more evenly and fill the reservoir pore space more effectively, leading to a significant overall pressure increase. As the hydrogen storage cycles progress, hydrogen gradually becomes the dominant component in the reservoir, and the influence of cushion gas types diminishes.

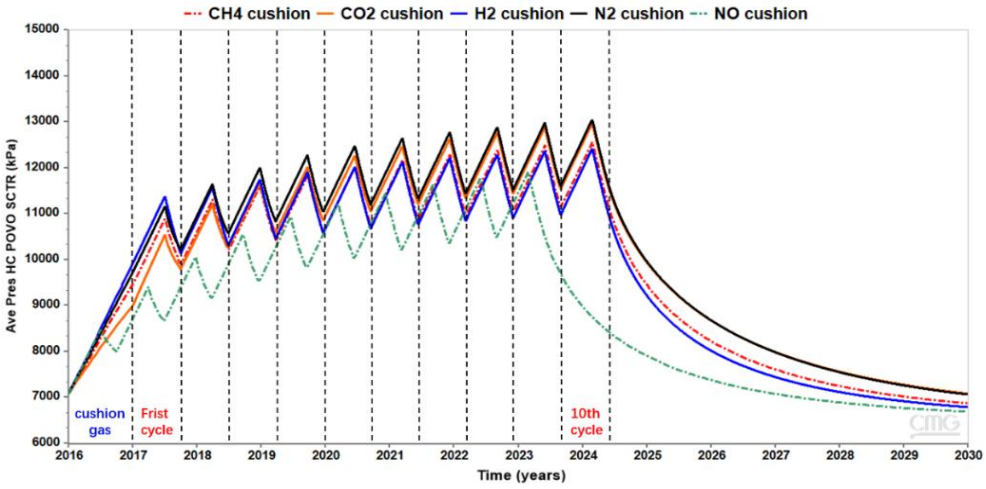

Figure 9—Effect of different cushion gas on reservoir pressure.

Figure 10 illustrates the impact of different cushion gases on the cumulative H_2 injection and production volumes. The results indicate that when H_2 is used as a cushion gas, the cumulative injection of H_2 is the highest. However, the cumulative H_2 production in the 10th cycle and the final cumulative production are relatively low, resulting in H_2 recovery rates of only 76.49% and 92.87% respectively. This indicates that H_2 is not an ideal cushion gas because the H_2 used as a cushion gas is also included in the cumulative injected volume, representing a waste of H_2. Therefore, selecting more cost-effective and readily available gases as cushion gases is more appropriate. When N_2, CH_4, or CO_2 is used as a cushion gas, both the 10th cycle and final cumulative H_2 production increase, leading to significant improvements in H_2 recovery rates. These results are like the performance of cushion gases in Figure 10, indicating that N_2 and CH_4 are better suited as cushion gases for H_2 storage (**Table 8**).

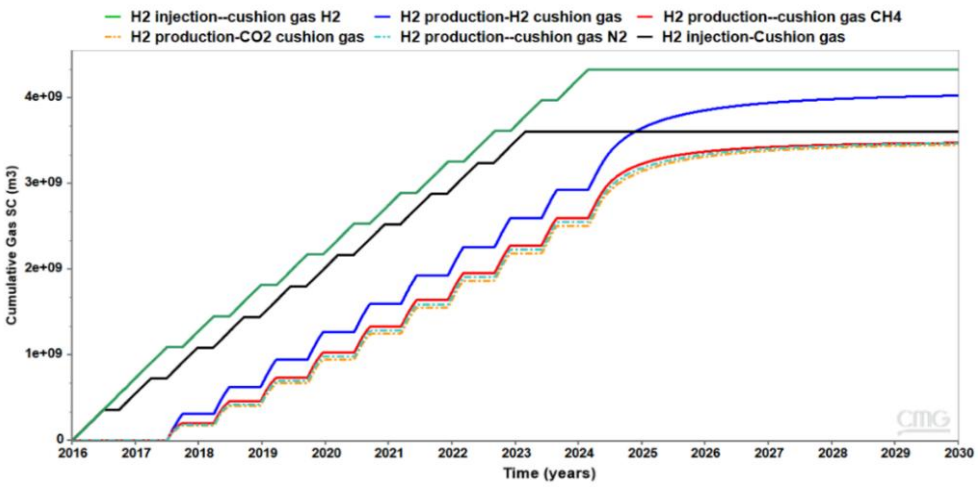

Figure 10—Effect of different cushion gas on H_2 cumulative injection and production.

Table 8—Effect of different cushion gas on H_2 recover.

Cushion gas type	10th cycle		Ultimate time	
	CHP ($10^8 m^3$)	RF (%)	CHP ($10^8 m^3$)	RF (%)
No cushion gas	26.92	74.36	33.36	92.15
H_2 cushion gas	33.92	76.49	40.25	92.87
N_2 cushion gas	29.85	82.4	34.70	95.85
CH_4 cushion gas	30.34	83.12	34.74	95.96
CO_2 cushion gas	29.31	80.97	34.52	95.36

(CHP: cumulative H_2 production; RF: H_2 recovery; Ultimate time: 7-year depletion phase following the final cycle)

Injection Rate. To investigate the effects of different injection rates on underground hydrogen storage, five sets of different scenarios were compared. To maintain a constant total volume of injected H_2 (**Figure 11**), injection rates were set at 0.5×10^6,1.0×10^6, 1.5×10^6, 2.0×10^6, and 2.5×10^6 m^3/day (with corresponding decreases in the injection-production cycle time).

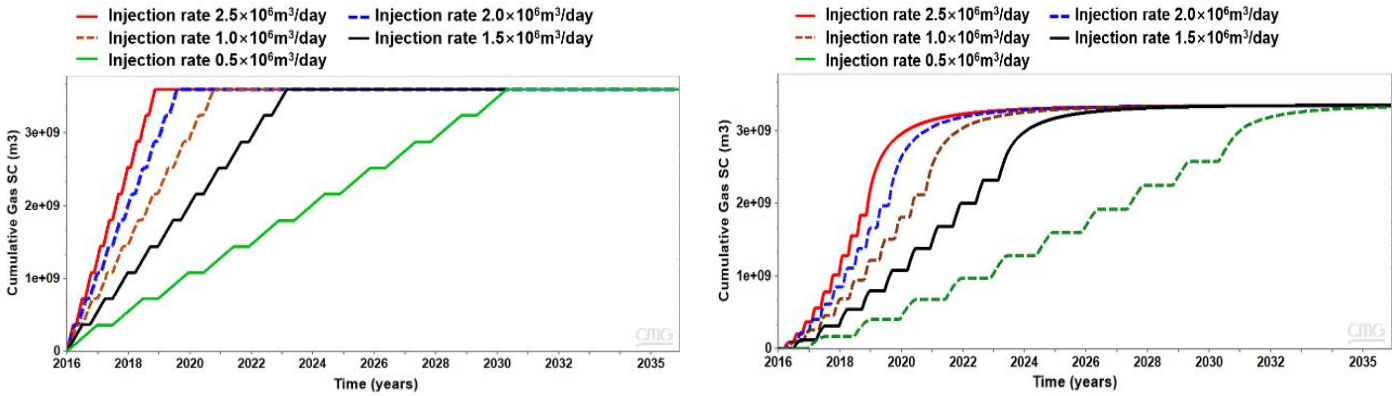

(a) Cumulative H_2 injection (b) Cumulative H_2 production

Figure 11—Effect of different injection rates on H_2 cumulative injection and production.

As shown in **Figure 12**, an increase in injection rate leads to a corresponding rise in reservoir pressure. However, this results in a decrease in CH_4 purity and an increase in H_2 purity within the produced gas. When the injection rate reaches 2.5×10^6 m^3/day, the reservoir pressure can hit 14 MPa. Although the purity of produced H_2 is high, the H_2 recovery rate at the end of the cycle is low. This is primarily due to the dual-well, inject-produce model used, where rapid pressure increases caused by high-rate H_2 injection led to H_2 predominantly accumulating near the injection well, without sufficient time to disperse to the farther reaches of the reservoir.

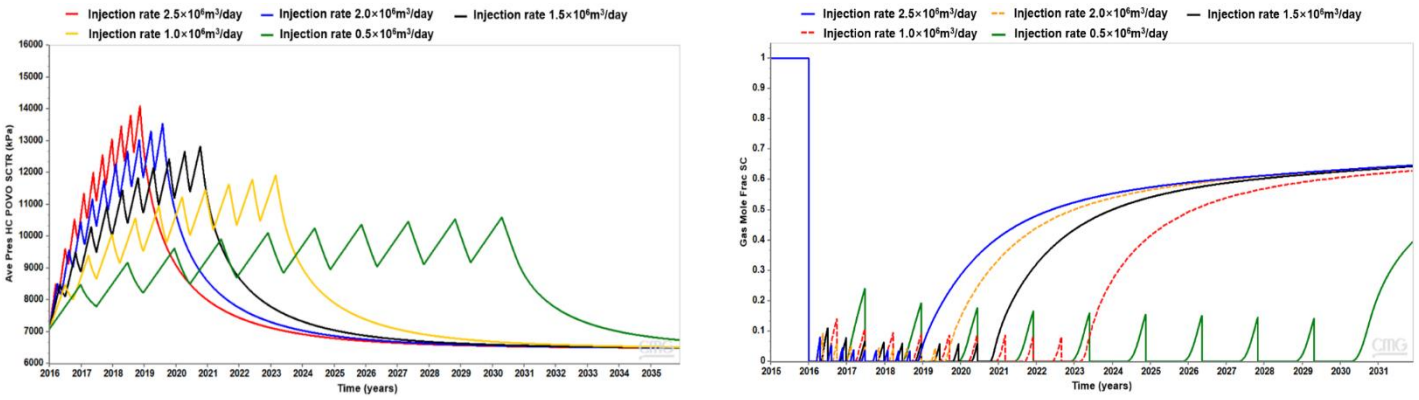

(a)Injection rates vs. reservoir pressure (b)Injection rates vs. mole fraction

Figure 12—Effect of different injection rates

Additionally, while the pressure inside the reservoir quickly builds to a high level at high injection rates, the rapid pressure decline following cessation of injection is detrimental to effective H_2 recovery. Consequently, although reservoir pressure peaks and natural gas production quickly increases after stopping the injection, as production continues, reservoir pressure begins to decline, eventually stabilizing the H_2 recovery rate at 92.15% (**Table 9**). This demonstrates that while the injection and production rates do not affect the final H_2 recovery in the storage process, they do influence the rate and efficiency of achieving this recovery.

Table 9—Effect of different injection rates on H_2 recovery.

Injection rate, （$\times10^6m^3$/day）	10th cycle		Ultimate time	
	CHP (10^8m^3)	H_2 RF (%)	CHP (10^8m^3)	H_2 RF (%)
0.5	29.10	80.38	33.36	92.15
1.0	26.92	74.36	33.36	92.15
1.5	24.31	67.15	33.36	92.15
2.0	22.73	67.15	33.36	92.15
2.5	21.92	60.55	33.36	92.15

(CHP: cumulative H_2 production; H_2 RF: H_2 recovery; Ultimate time: 7-year depletion phase following the final cycle)

Injection-production Cycle. To investigate the impact of different H_2 injection-production cycle counts on underground hydrogen storage efficiency, this study established four groups with varying cycle counts: 5, 10, 15, and 20 cycles. To maintain a consistent total volume of injected H_2, the duration of each cycle was reduced as the number of cycles increased.

As shown in **Figure 13**, fewer cycles result in a greater amount of H_2 injected per cycle, thereby leading to higher reservoir pressures. **Figure 14** and **Table 10** display the cumulative volumes of H_2 injected and produced under different cycle counts, along with the corresponding H_2 recovery rates. The results indicate that although the variation in cycle counts has a minimal impact on the amount of H_2 stored, higher cycle counts lead to relatively higher H_2 recovery rates.

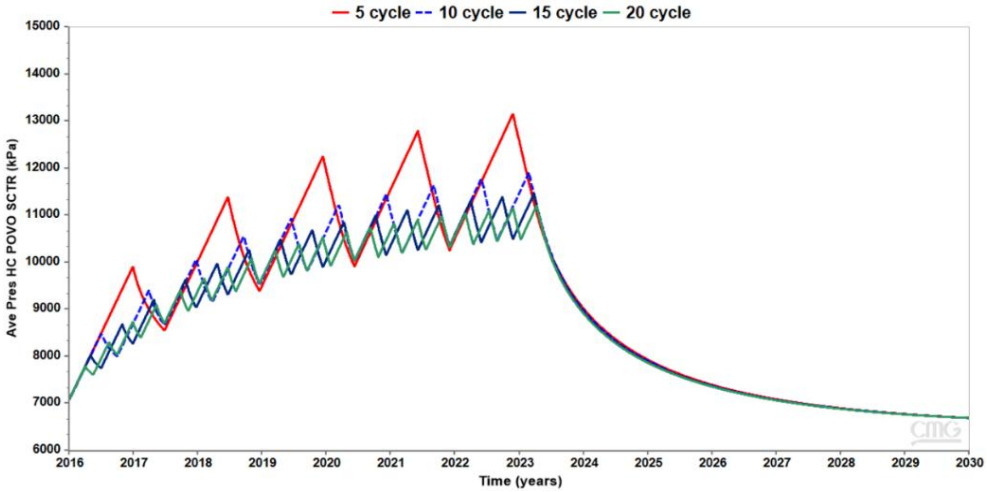

Figure 13—Effect of different numbers of cycles on reservoir pressure.

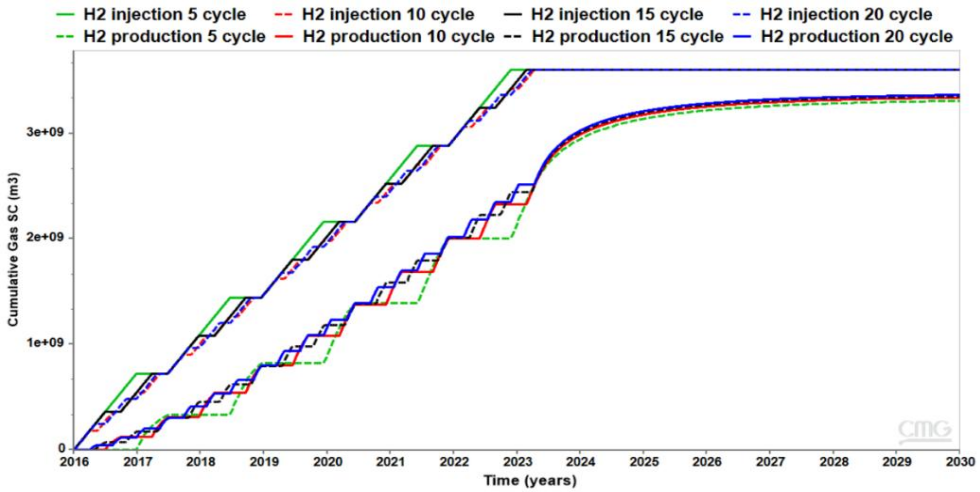

Figure 14—Effect of different numbers of cycles on H_2 cumulative injection and production.

Table 10—Effect of different numbers of cycles on H_2 recovery.

Injection-production cycle (Cycles)	10th cycle		Ultimate time	
	CHP (10^8m^3)	H_2 RF (%)	CHP (10^8m^3)	H_2 RF (%)
5	26.73	73.84	33.01	91.18
10	26.92	74.36	33.36	92.15
15	27.18	72.08	33.47	92.45
20	27.23	75.22	33.58	92.76

(CHP: cumulative H_2 production; RF: H_2 recovery; Ultimate time: 7-year depletion phase following the final cycle)

Figure 15 illustrates the molar fractions of in the gas produced under different cycle counts. With an increase in cycle counts, the purity of in the produced gas decreases, while the purity of H_2 increases. This is because fewer cycles mean more H_2 is injected per cycle, significantly increasing the initial reservoir pressure. This higher initial pressure leads to increased CH_4 production, subsequently affecting the purity of H_2. Overall, these findings suggest that increasing the cycle count can optimize the purity and recovery rates of H_2, which is crucial for enhancing the economic benefits and efficiency of underground hydrogen storage.

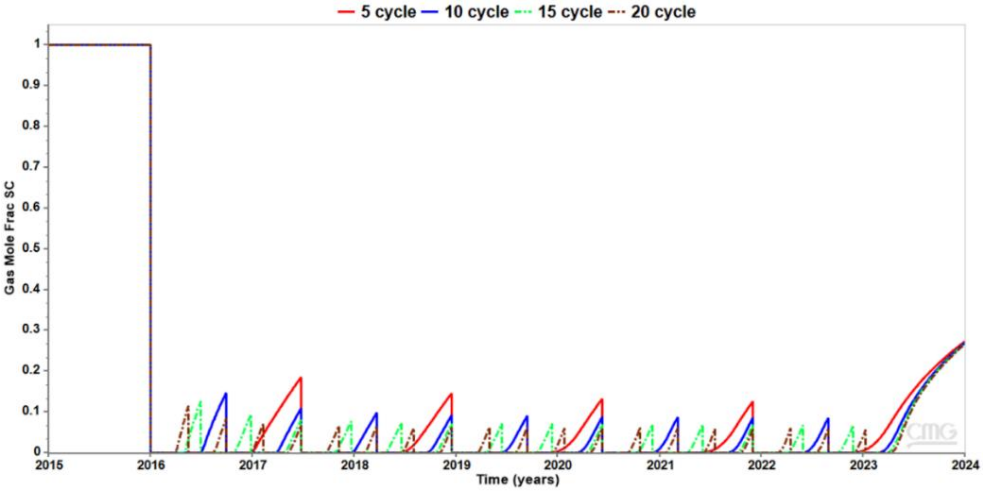

Figure 15—Mole fraction of CH_4 in different numbers of cycles.

Diffusion Effect. To investigate the impact of H_2 molecular diffusion on underground hydrogen storage, we established a control group for molecular diffusion simulation. **Figure 16** shows the influence of considering H_2 molecular diffusion on the cumulative injection and production of H_2 in the reservoir. The results indicate that molecular diffusion does have some effect on H_2 storage, though the impact is not significant and is mainly due to the high injection rate.

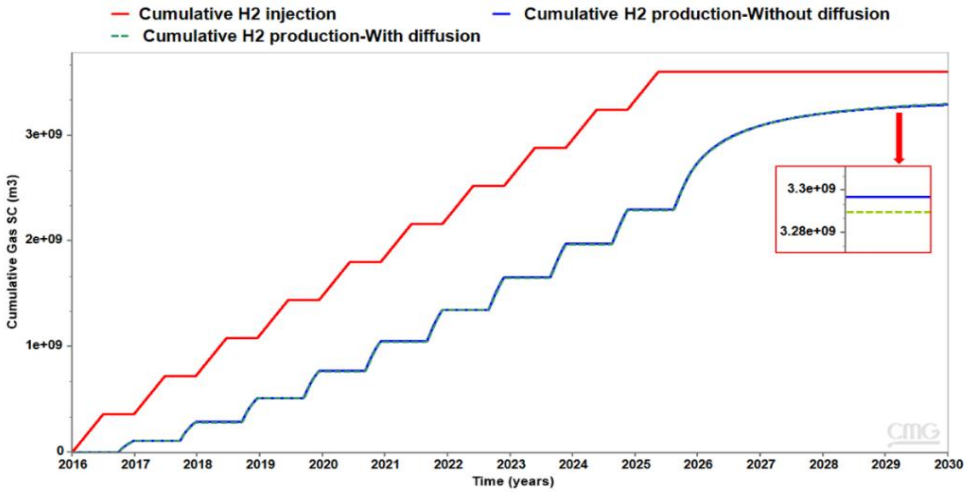

Figure 16—Effect of molecular diffusion on H_2 cumulative injection and production.

Consequently, we simulated a control group with a lower rate of molecular diffusion. As shown in **Figure 17**, molecular diffusion at lower rates does not have a beneficial effect on H_2 recovery. Compared to scenarios without diffusion, considering molecular diffusion can reduce H_2 recovery by up to 3.3% (**Table 11**). This is

because molecular diffusion is a fundamental mass transfer phenomenon where H_2 is lost to the reservoir by diffusing into the water, leading to reduced H_2 production and recovery.

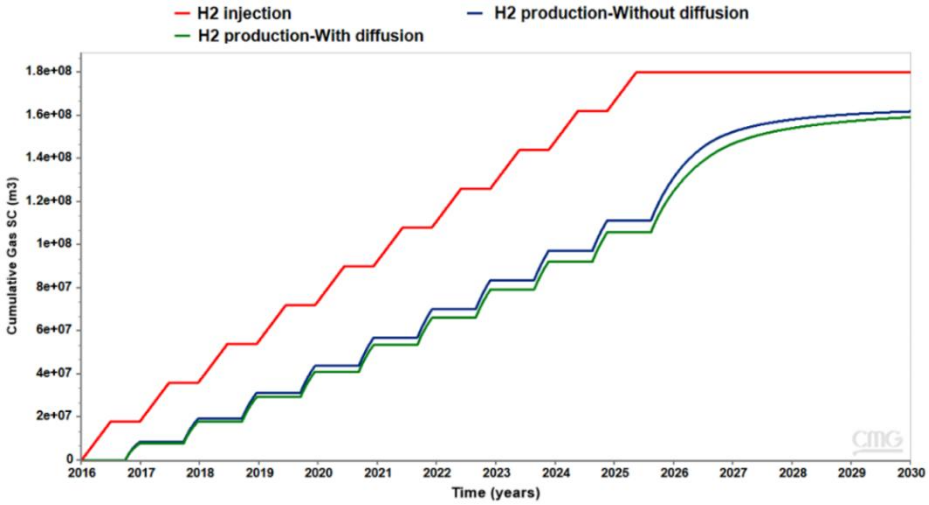

Figure 17—Effect of molecular diffusion on H_2 cumulative injection and production with lower injection rate.

Table 11—Effect of molecular diffusion on H_2 recovery.

Diffusion	10th cycle		Ultimate time	
	CHP ($10^8 m^3$)	H_2 RF (%)	CHP ($10^8 m^3$)	H_2 RF (%)
With diffusion	1.25	69.44	1.58	87.77
Without diffusion	1.31	72.77	1.62	90.00

(CHP: cumulative H_2 production; RF: H_2 recovery; Ultimate time: 7-year depletion phase following the final cycle)

Furthermore, the impact of gas diffusion is not only evident in the loss of H_2 to the reservoir but also affects the purity of the produced H_2 due to its mixing with existing gases. As illustrated in **Figure 19**, at lower H_2 injection rates, the impact of molecular diffusion on the mole fraction of H_2 in the produced gas is clearly visible. The results show that considering diffusion effects significantly decreases the purity of H_2 in the produced gas.

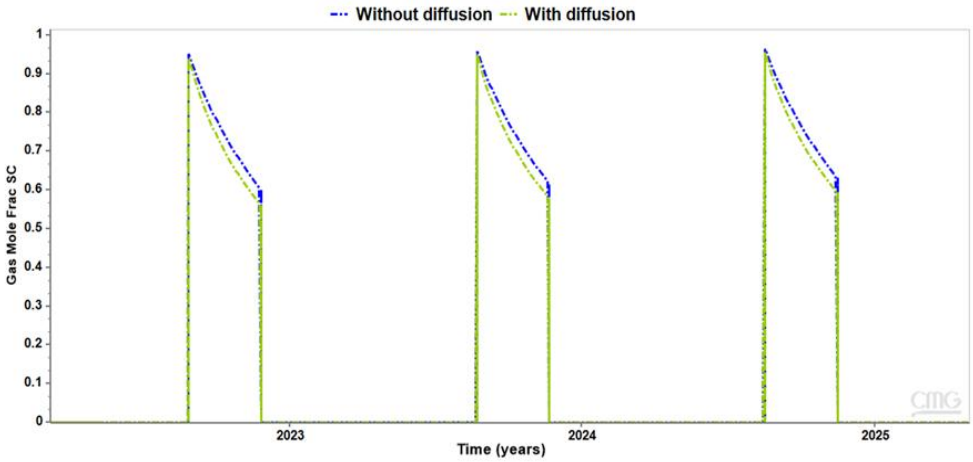

Figure 19—Effect of molecular diffusion on the mole fraction of H_2 in the produced gas with lower injection rate.

Figure 20 displays the distribution of H_2 in the reservoir after the 10th cycle, including both scenarios with and without molecular diffusion. Different colors represent different H_2 concentrations, with white areas indicating rock media where H_2 cannot be stored. Clearly, the H_2 concentration near the well is higher. Furthermore, as shown in Figure 20b, when molecular diffusion is considered, the distribution of H_2 in the reservoir becomes more widespread, allowing it to further diffuse from the vicinity of the well, especially into areas with higher porosity and permeability. This diffusion is a key factor influencing underground hydrogen storage performance. Therefore, the feasibility studies of underground hydrogen storage should fully consider the molecular diffusion of H_2.

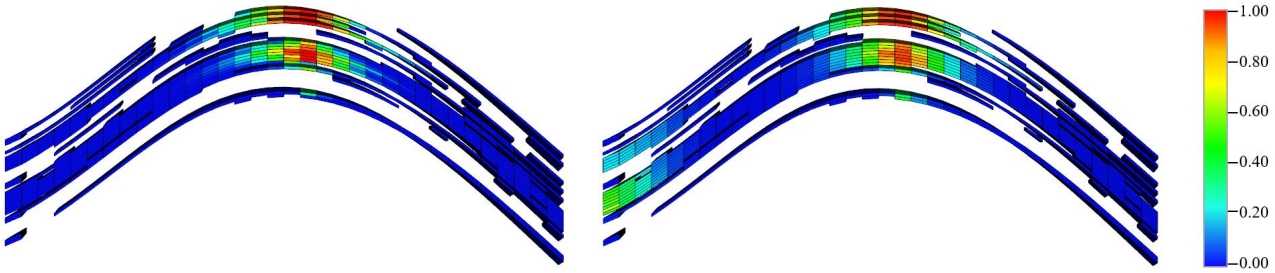

(a)Without diffusion (b)With diffusion

Figure 20—Effect of molecular diffusion on H_2 molar fraction in the reservoir.

Conclusions

This study investigated the feasibility of underground hydrogen storage in depleted gas reservoirs. Numerical simulations based on a pure methane fluid model were performed for the underground hydrogen storage process consisting of 16 years of depletion followed by 10 cycles (7 years) of H_2 injection and production, with an additional 7-year extended production phase. Furthermore, to analyze the influencing factors during the underground hydrogen storage process, sensitivity analyses were conducted on different injection timings, injection rates, injection-production cycles, cushion gas types, and molecular diffusion. The main conclusions drawn from this study are as follows:

1. Depleted gas reservoirs prove to be a relatively ideal option for underground hydrogen storage. At the end of 10 injection-production cycles, the H_2 recovery reaches 74.36%. The final H_2 recovery can also reach 92.15%
2. The timing of H_2 injection is crucial. Injecting H_2 earlier results in lower H_2 purity in the produced gas, but a higher H_2 recovery.
3. Using N_2 as cushion gas during the underground hydrogen storage process leads to higher reservoir pressure and increased H_2 recovery.
4. The injection-production cycle has almost no impact on H_2 recovery. Higher injection rates result in lower H_2 purity and lower recovery.
5. Molecular diffusion is detrimental to underground hydrogen storage. At higher H_2 injection rates, the impact of molecular diffusion on H_2 storage is relatively low. However, reducing the H_2 injection rate results in reduced H_2 recovery and purity due to molecular diffusion.

The findings of H_2 storage in depleted gas reservoirs have certain limitations and may not be directly applicable to H_2 storage in salt caverns or aquifers due to the significant differences in the physical properties and behavior of these reservoirs. Furthermore, although this study has considered various engineering factors affecting H_2 storage performance, it has not fully accounted for potential loss mechanisms during long-term storage. For instance, chemical reactions between H_2 and reservoir rocks may lead to changes in porosity, while microbial activity could consume H_2 or produce byproducts over extended periods. These long-term dynamic effects require further investigation to refine the storage model and enhance its practical applicability.

Conflicting Interests

The author(s) declare that they have no conflicting interests.

References

Zhu, Y. 2021. Scenario Planning and Environmental Benefits Study for China's Future Energy System with High Proportions of Renewable Energy. Master's Thesis, Huazhong University of Science and Technology, Hefei, China.

Noussan, M., Raimondi, P. P., Scita, R., et al. 2021. The Role of Green and Blue Hydrogen in the Energy Transition-A Technological and Geopolitical Perspective. *Sustainability* **13**(1): 298.

Bauer, S., Beyer, C., Dethlefsen, F., et al. 2013. Impacts of the Use of the Geological Subsurface for Energy Storage: An Investigation Concept. *Environmental Earth Sciences* **70**(1): 3935-3943.

Wang, L., Jin, Z., Lv, Z., et al. 2024, Hydrogen Storage in Gas Reservoirs: A Molecular Modeling and Experimental Investigation. *Earth Science* **49**(6):2044-2057.

Gabrielli, P., Poluzzi, A., Kramer, G. J., et al. 2020. Seasonal Energy Storage for Zero-Emissions Multi-Energy Systems via Underground Hydrogen Storage. *Renewable and Sustainable Energy Reviews* **121**(1): 109629.

Shao, Z. and Yi, B. 2019. Developing Trend and Present Status of Hydrogen Energy and Fuel Cell Development. *Bulletin of Chinese Academy of Sciences* **34**(4): 469-477.

Li, J., Zhou, M., Zhu, L., et al. 2021. Flexibility Requirement Quantifying and Optimal Dispatching for Renewable Integrated Power Systems. *J Power System Technology* **45**(7): 2647-2656.

Shi, Z., Jessen, K., and Theodore, T. T. 2020. Impacts of the Subsurface Storage of Natural Gas and Hydrogen Mixtures. *International Journal of Hydrogen Energy* **45**(15): 8757-8773.

Züttel, A. 2003.Materials for Hydrogen Storage. *Materials today* **6**(9): 24-33.

Züttel, A. 2004. Hydrogen Storage Methods. *Naturwissenschaften* **91**(1): 157-172.

Zhou, L. 2005. Progress and Problems in Hydrogen Storage Methods. *Renewable and Sustainable Energy Review* **9**(4): 395-408.

Demirel, Y. 2012. *Energy: Production, Conversion, Storage, Conservation, And Coupling*. New York City: Springer Cham.

Hagemann, B., Ganzer, L., and Panfilov, M. 2018. Field Scale Modeling of Bio-Reactions During Underground Hydrogen Storage. Paper presented at the 16th European Conference on the Mathematics of Oil Recovery, Barcelona, Spain, 3-6 September.

Thoraval, A., Lahaie, F., Brouard, B., et al. 2015. A Generic Model for Predicting Long-Term Behavior of Storage Salt Caverns after Their Abandonment as an Aid to Risk Assessment. *International Journal of Rock Mechanics and Mining Sciences* **77**(1): 44-59.

Michalski, J., Bünger, U., Crotogino, F., et al. 2017. Hydrogen Generation by Electrolysis and Storage in Salt Caverns: Potentials, Economics and Systems Aspects with regard to the German Energy Transition. *International Journal of Hydrogen Energy* **42**(19): 13427-13443.

Ozarslan, A. 2012. Large-scale Hydrogen Energy Storage in Salt Caverns. *International journal of hydrogen energy* **37**(19): 14265-14277.

Feldmann, F., Hagemann, B., Ganzer, L., et al. 2016. Numerical Simulation of Hydrodynamic and Gas Mixing Processes in Underground Hydrogen Storages. *Environmental Earth Sciences* **75**(1):1165.

Kanaani, M., Sedaee, B., and Asadian-Pakfar, M. 2022. Role of Cushion Gas on Underground Hydrogen Storage in Depleted Oil Reservoirs. *Journal of Energy Storage* **45**(1): 103783.

Amid, A., Mignard, D., and Wilkinson, M. 2016. Seasonal Storage of Hydrogen in a Depleted Natural Gas Reservoir. *International journal of hydrogen energy* **41**(12): 5549-5558.

Tarkowski, R. 2019. Underground Hydrogen Storage: Characteristics and Prospects. *Renewable and Sustainable Energy Reviews* **105**(1):86-94.

Zamehrian, M. and Sedaee, B., 2022. Underground Hydrogen Storage in a Naturally Fractured Gas Reservoir: The Role of Fracture. *International Journal of Hydrogen Energy* **47**(93): 39606-39618.

Lemieux, A., Shkarupin, A., and Sharp, K. 2020. Geologic Feasibility of Underground Hydrogen Storage in Canada. *International Journal of Hydrogen Energy* **45**(56): 32243-32259.

Hemme, C. and Van Berk, W. 2018. Hydrogeochemical Modeling to Identify Potential Risks of Underground Hydrogen Storage in Depleted Gas Fields. *Applied Sciences* **8**(11): 2282.

Lysyy, M., Fernø, M., and Ersland, G. 2021. Seasonal Hydrogen Storage in a Depleted Oil and Gas Field. *International Journal of Hydrogen Energy* **46**(49): 25160-25174.

Carchini, G., Hamza, A., Hussein, I. A., et al. 2023. Hydrogen Storage in Gas Reservoirs: A Molecular Modeling and Experimental Investigation. *Hydrogen Energy* **48**(20): 7419-7430.

Chai, M., Chen, Z., Nourozieh, H., et al. Numerical Simulation of Large-Scale Seasonal Hydrogen Storage in An Anticline Aquifer: A Case Study Capturing Hydrogen Interactions and Cushion Gas Injection. *Applied Energy* **334**(6396): 120655.

Song, H., Zhou, Y., Xie, Z., et al. 2024. A Pore-Scale Simulation of the Effect of Heterogeneity on Underground Hydrogen Storage. *Water* **16**(22): 3264.

Mei, L. 2011. Characteristics of Water Bearing Formation and Gas Water Distribution Control Factors in Gas Reservoir He 8 of Sulige Gas field, Ordos Basin. *Environmental Science* **24**(1):248-252.

Reuß, M., Grube, T., Robinius, M., et al. 2017. Seasonal Storage and Alternative Carriers: A Flexible Hydrogen Supply Chain Model. *Applied energy* **200**(1): 290-302.

Pan, B., Xin, Y., Ju, Y., et al. 2021. Underground Hydrogen Storage: Influencing Parameters and Future Outlook. *Advances in Colloid and Interface Science* **294**(1): 102473.

Xueling Ma, is a master candidate in Petroleum Engineering department at Xi'an Shiyou University. She has focused her research on areas involving CCUS, reservoir simulation and enhance oil recovery.

Lu Zou, is a master candidate in Petroleum Engineering department at Xi'an Shiyou University. He has focused his research on areas involving reservoir simulation and enhance oil recovery.

Zhanrong Yang, is a master candidate in Petroleum Engineering department at Xi'an Shiyou University. He has focused his research in areas involving reservoir simulation and enhance oil recovery.

Tong Hou, is a master candidate in Petroleum Engineering department at Xi'an Shiyou University. She has focused her research on areas involving reservoir simulation and enhance oil recovery.

Weirong Li, is a Professor in the Petroleum Engineering Department at Xi'an Shiyou University. His research interests include unconventional resources/reserves estimates, reservoir simulation, well testing, and production analysis. Dr. Li holds a bachelor's degree in petroleum engineering from Northeast Petroleum University, China; a master's degree in petroleum engineering from Research Institute of Petroleum Exploration and Development, China; and a PhD degree in petroleum engineering from Texas A&M University.

Keze Lin, is an undergraduate student at China University of Petroleum (Beijing), majoring Petroleum Engineering.

Hongliang Yi, is a senior reservoir engineer in Liaohe Oilfield Company of PetroChina. He specializes in enhanced oil recovery.

Zhilong Liu, is a senior reservoir engineer in EnerTech-Drilling & Production Co., CNOOC Energy Technology & Services Limited, Tianjin, China. He specializes in enhanced oil recovery.